

Three-Dimensional, Unsteady, Inviscid Flow in an Axial Turbine Stage

Dr. Abdulhassan A. Karamallah*, Dr. Talib Z. Farge** & Dr. Sudad I. Younis***

Received on: 4/9/2006

Accepted on: 4/12/2008

Abstract

This paper presents an advanced approach to compute the three-dimensional, rotational, adiabatic, inviscid flow of a perfect gas in a highly twisted transonic axial turbine stage. The time-dependent Euler equations, expressed in a Cartesian coordinate system, are solved using a time marching method and a finite volume approach. The absolute flow is computed in the nozzle vanes passage, whereas the relative flow is computed in the rotor blades passage. The phase relation of nozzle and rotor flows and the related blade row interaction are accounted for in the time-space domain. The results show that the present method of calculation makes a practical contribution to predict actual turbine flows through a turbine stage that have an arbitrary number of vanes and blades for each nozzle and rotor. It is clear that this flow has a three dimensional aspects, in spite of the high hub/tip ratio which has theoretically a two-dimensional flow aspects.

Keywords: 3-D unsteady inviscid flow, axial turbine stage, nozzle-rotor interaction.

حساب الجريان الغير منتظم الثلاثي البعد و غير اللزج في مرحلة التوربين المحوري

الخلاصة

يقدم هذا البحث طريقة متقدمة لحساب الجريان الأديباتي الدوراني الغير لزج و الثلاثي البعد لغاز مثالي في مرحلة التوربين المحوري عن طريق حل معادلات الحركة (اويلر) المعبر عنها بالإحداثيات الديكارتية باستخدام طريقتي مسار الوقت و الحجم المحدد. تم إجراء الحسابات باستخدام خصائص الجريان المطلقة لقناة الريش الثابتة بينما أجريت الحسابات باستخدام خصائص الجريان النسبية لقناة الريش الدوارة. تم اخذ العلاقة الطورية وتداخل صفوف الريش بنظر الاعتبار في حقل الزمن و الفراغ. بينت النتائج بأن الطريقة في الحسابات تقدم مساهمة عملية في تخمين الجريان الحقيقي خلال التوربين لمرحلة توربين محوري ذات عدد عشوائي من الريش لكل من الريش الثابتة و الدوارة. كذلك تبين بوضوح بأن الجريان خلال مرحلة التوربين له خصائص ثلاثية البعد بالرغم من النسبة العالية لنصف قطر الريشة إلى نصف قطر نهايتها والتي يكون الجريان فيها ثنائي البعد نظريا.

1. Introduction

The flow in an axial turbine stage is very complex, the flow is unsteady, three-dimensional, has regions where viscous effect is important and has interaction effect between the nozzle and the rotor. The solution of the full three-dimensional equations of motion with full boundary conditions represents a difficult task both from a computational and modeling point of view [1]. Many

numerical methods have been proposed and developed for the calculation of the blade-to-blade flows in turbomachinery, only a few have survived [2].

The flow of fluid, which causes the dynamic action of blades, can be calculated by many (CFD) methods. The flow in turbine passages could be either subsonic and/or supersonic, with or without shock depending on the operating conditions.

* Mechanical Engineering Department, University of Technology/ Baghdad

** Department of Materials Engineering, University of Technology/ Baghdad

*** Laser and Optoelectronics Engineering Department, University of Technology/ Baghdad

The appropriate method to predict such flows and currently satisfy the design criteria and analysis tasks is the time marching method, since these methods are accurate, stable computationally, efficient and capable of treating the broad range of airfoil geometries and conditions in modern turbomachinery [3].

The present work is based on the solution of the unsteady three-dimensional Euler equations by using the time marching method and finite volume approach to calculate the flow in an axial turbine stage.

The flow field is divided into two regions, the nozzle passage region and the rotor passage region. Both passages are extended upstream and downstream, each region will be divided into grid network taking into account at least one cell at the upstream of the rotor that must coincide with one cell at the downstream of the nozzle at the mid plane of axial gap. Then different terms in the Euler equations are to be defined at each grid point. The phase relation of nozzle and rotor flows and the related blade row interaction are accounted in the time-space domain.

The flow field can be solved from the Euler equation in finite volume integral form subjected to the imposed boundary conditions. Flow calculations will be done using finite volume cell structure with the flow variables stored at each center of the cells [4].

The flow through the turbine stage is firstly treated as two-dimensional at three sections namely at hub, mid and tip sections for both stator and rotor cascades and the resultant flow properties will be taken as initial guess for the three-dimensional solution, so that the number of iterations and the computational time to achieve the steady state solution will be reduced.

2. Principle of Stage Calculation

The flow through two successive blade rows in relative motion is basically unsteady [5]. The

boundary conditions of the present problem, downstream of the nozzle and upstream of the rotor, are not known, as they are part of the solution. The mean interaction between vanes and blades is achieved by repeatedly adapting these boundary conditions to the evolution of the flow pattern until stabilization and correspondence of mass flow in both blade passages is achieved for each phase location of the rotor.

3. Governing Equations

For axial turbine stage flow calculations, absolute velocities and a fixed frame of reference are considered in the stator, whereas in the rotor it was decided to work with velocities and a coordinate system rotating at the blade angular velocity Ω around the x-axis, coinciding with the machine axis. The strong conservation form of the unsteady, three-dimensional Euler equations in Cartesian coordinates can be written in non-dimensional variables as [6]

$$\frac{\partial F}{\partial t} + \frac{\partial G}{\partial x} + \frac{\partial H}{\partial y} + \frac{\partial I}{\partial z} = B \quad (1)$$

where,

$$F = \begin{bmatrix} r \\ ru \\ rv_r \\ rw_r \\ rE \end{bmatrix}, G = \begin{bmatrix} ru \\ ru^2 + p \\ ruv_r \\ ruw_r \\ u(rE + p) \end{bmatrix}, H = \begin{bmatrix} rv \\ ruv \\ rvv_r + p \\ rvw_r \\ v(rE + p) \end{bmatrix}$$

$$I = \begin{bmatrix} rw \\ ruw \\ rvw_r \\ rvw_r + p \\ w(rE + p) \end{bmatrix}, B = \begin{bmatrix} 0 \\ 0 \\ \Omega rv \\ -\Omega rw \\ 0 \end{bmatrix} \quad (2)$$

where r is the density, p is the static pressure, (u, v, w) are the absolute velocity components in the x, y, z

directions, respectively, (v_r, w_r) are the relative velocity (absolute for stator, $\Omega=0$) components in the y, z directions respectively. And these are given by,

$$v_r = v - \Omega z \tag{3}$$

$$w_r = w + \Omega y \tag{4}$$

The definition of the total energy E gives the additional relation [7]

$$E = cvT + \frac{W^2}{2} - \frac{\Omega^2 r^2}{2} \tag{5}$$

where, W is absolute velocity in stator and relative velocity in rotor.

Using the perfect gas law and the definition of total absolute and relative energy, Eq.(1) is completed by the following relation

$$p = (\gamma - 1) \rho \left\{ E - \frac{W^2}{2} + \frac{\Omega^2 r^2}{2} \right\} \tag{6}$$

where, γ is the ratio of specific heat.

4. Grid and Computational Domain

A simple grid system of finite volume elements is adopted, considering one blade passage each for stator vanes and rotor blades. A three-dimensional view of the turbine stage computational domain including the four selected positions of rotor phase is illustrated in Fig.(1). The mesh size is not arbitrary since the number of stationary vanes and rotating blades are not equal. The selection of mesh size must satisfy that at least one grid cell is overlapped in the axial direction for each of the rotor phase location at the interface between the nozzle vanes row and the rotor blades row.

The mesh grid configuration with trapezoidal element for the stage of rotor at phase (I) location is shown in Fig. (2).

5. Numerical Scheme

The central difference version of finite volume method applied to Euler equation (1) may be written as

$$\bar{U}^{n+1} = \bar{U}^n + \frac{\Delta t}{\Delta vol} \sum_{faces} \left(\begin{matrix} transport \\ term \end{matrix} \right)^n \tag{7}$$

Where,

\bar{U} is the property matrix,

n at time t ,

$n+1$ at time $t+\Delta t$.

The transport terms have to be taken as positive for transport into the element and negative for a transport out of the element. These terms are computed at the cell faces assuming that there are linear variation between the element centers.

Numerical stability is ensured by introducing a non-derivative term namely a damping term in the partial differential equations. The second order accuracy damping term for the velocity component in x -direction (u) is given by [8]

$$D_u(ijk)^{n+1} = \frac{A}{6} [u_{i1,jk} + u_{i2,jk} - 2u_{ijk}] + \frac{A}{6} [u_{ij1k} + u_{ij2k} - 2u_{ijk}] + \frac{A}{6} [u_{ijk1} + u_{ijk2} - 2u_{ijk}] \tag{8}$$

where,

A is a damping factor generally less than one,

$i1, j1, k1$ are $i+1, j+1, k+1$ node respectively,

$i2, j2, k2$ are $i-1, j-1, k-1$ node respectively.

The presence of the damping terms must not be allowed to contaminate the second order accuracy of the converged, time-steady solution, so a correction term \overline{CF} is added at the explicit time level to ensure that,

$$\overline{CF}^n = (1 - RF) \cdot \overline{CF}^{n-1} - RF \cdot \overline{D}^n \tag{9}$$

The relaxation term for velocity component (u) is therefore,

$$\overline{CF}_u^n = (1 - RF) \cdot \overline{CF}_u^{n-1} - RF \cdot \overline{D}_u^n \tag{10}$$

where RF is the relaxation factor whose value is typically 0.05 [9].

The final equation of the new velocity component (u) become

$$u^{n+1} = u^n + \frac{M_x^{n+1}}{r^{n+1}} \cdot \frac{\Delta t}{\Delta vol} + D_u^{n+1} + CF_u^n \quad (11)$$

where M_x is the summation of flux of momentum across the cell faces.

In the same way the numerical scheme of eqns. (8, 10, 11) can be written for (r, v, w, v_r, w_r, E).

At a time-steady solution $\bar{F} \rightarrow 0$, $\bar{CF} \rightarrow -\bar{D}$ and hence the desired result is obtained and the fluid properties satisfy

$$r^{n+1} = r^n, u^{n+1} = u^n, v^{n+1} = v^n, w^{n+1} = w^n \\ v_r^n = v_r^{n+1}, w_r^n = w_r^{n+1}, To^{n+1} = To^n \text{ and } p^{n+1} = p^n.$$

For a partial differential equations system with three or four independent variables (x, y, z and t), the Courant-Friedrichs-Lewy (CFL) stability condition can be used. The CFL stability condition states that the distance covered during the time interval Δt by the disturbance propagating with speed (a) should be less than one [10].

It is more practical to use the simplified relation [11]

$$\frac{1}{\sqrt{g}}(c+a)\frac{\Delta t}{\Delta l} \leq 1 \quad (12)$$

where a is the speed of sound.

The numerical solution shows good agreement with the predicted stability limit in choosing the time steps.

6. Boundary Conditions

In order to have a well-posed problem, system of equations must be completed with a set of boundary conditions. The solution must be subjected to the following restrictions. At (t=0), the initial guess can be completely arbitrary, as the final asymptotic solution is independent of the initial guess. The

initial conditions affect only the total time taken for convergence.

In the inlet plane of the stage, the total temperature, total pressure and the flow angles are specified from the operational condition of the axial turbine stage. This set of conditions is most generally used for turbomachinery flow calculations. At the inlet of the rotor passage, the properties obtained from the outlet of the nozzle passage are converted to the relative values in order to determine the rotary stagnation properties and reduced static pressure needed in the solution of energy equation through the rotor.

In the outlet plane of the stage, the static pressure is specified from the operational condition and held constant and the velocity is completely axial since the studied condition is axial flow turbine stage. At the outlet boundary of the nozzle passage, the flow properties are calculated from the isentropic relations and since these properties are not known at the beginning of the calculation, hence their spanwise distribution is repeatedly updated.

The same must be done for updating the relative properties at the upstream of the rotor cascade.

At the wall boundaries of each blade surfaces, there are no fluxes of mass and energy into the (ij)th cell across the wall and in the momentum. The force term is equal to the pressure at the wall multiplied by the projection area. The wall pressure is simply extrapolated from the first two interior cells neighboring the solid surfaces.

7. Results

Calculations were performed on a typical single-stage turbine with the present numerical scheme. The shape and grid configuration of the nozzle vane and rotor blade (phase I) at 50% span height used is shown in fig. (2). The description of stage geometry and test condition used

for the calculations is listed in table (1). The axial gap between the nozzle cascade and the rotor cascade is $\frac{1}{4}$ of the axial chord of the nozzle vane whereas the hub/tip ratio is 0.88. The stage has 62 vanes and 68 blades.

Before proceeding with the flow calculations in the turbine stage, a checking for the numerical scheme was made by taking a typical nozzle vane at mid span [12]. The pressure distributions on the suction and pressure surfaces that gained by the computer program is compared with the measurement performed in a wind tunnel and the comparison is shown in fig. (3). The results show that the predicted pressure distribution agrees well with the measurements and are closer than that predicted by the method described in [12].

For the simulation of the flow field for the nozzle vane passage, the mesh size without extensions is taken as (31x17x21) then extended upstream and downstream to be (39x17x21) fine grid. The integrated mesh size for the rotor passage is found to be (39x13x21) fine grid with extensions and this mesh size is similar for each rotor phase location. The typical CPU time was (125) seconds for about 500 iterations for convergence test of the nozzle passage flow calculations, while it was (120) seconds for about 300 iterations for convergence test of the rotor passage flow calculations. The reason of reaching convergence in the rotor passage flow calculations with less number of iterations than that in stator passage is due to the use of the energy equation in the solution of the flow in the rotor.

All flow properties can be computed using the present scheme, such as velocity components, density, total pressure and Mach number variations at any point in the flow field.

Fig. (4) shows the axial velocity contours and stream traces in selected planes in chord wise direction as

indicated. It is observed that there is a wake flow upstream the nozzle vanes passage due to the dual effect of low Mach number and vanes leading edge shape. Also there is a small reverse flow at a region close to the corner of hub zone due to the high bulb body at L.E and small spacing between the vanes at this region. This issue ended as the flow enters the passage but the secondary flow effect continues up to (0.167X/Ca) plane where the effect of blade geometry equals the pressure effect.

Fig. (5) represents the stator static pressure contours at the four phases of rotor location. It is clearly shown that the pressure at the pressure surface is higher than that at the suction surface and is not affected by the rotor rotation at (0.667X/Ca). At (0.8X/Ca) the rotor rotation effect appears especially at phase (III) location where a higher pressure drop occurred at the bottom half of the vane suction surface due to the higher sucking of the flow by the rotor at this phase. The same trend with smaller rate is observed at phase (IV). At the nozzle vane trailing edge the same issue can be observed with higher degree for phases (III and IV), while at phase (I and II) the rotor rotation effect appears with smaller degree. This effect continuously appears till the plane of interface between the nozzle and the rotor passages where a jet flow is observed at the region near the hub and a weak flow near the tip at phase (III), whereas a clear weak flow appears at the middle of the plane at phase (IV).

Fig. (6) represents the periodic static pressure distribution at mid span of the rotor passage. It can be seen from the figure that the convergence is good and obey the rule of that the pressure distribution follows the blade profile shapes and operating conditions. Also it can be seen that the static pressure has periodically little change along the pressure surface whereas this distribution

is approximately not changed along the suction surface and the pressure difference between the blade surfaces is increased with the rotor phase location, i.e., the phase (IV) that represents the phase at which the rotor passage completes one crossing of the stator passage with the ultimate pressure difference.

8. Conclusions

The numerical scheme has been presented for solution of the time-dependent Euler equations with application to unsteady, three-dimensional transonic flows in axial turbine stage passages. The method is computational explicit, possesses optimal damping characteristics and has a substantial computational speed advantage over other explicit methods. Numerical solution results for axial turbine cascade flows have been presented and compared with experimental data to demonstrate the validity, accuracy and computational efficiency of the analysis method in predicting the flow in axial turbine stage. The results prove that the flow in such stage has three-dimensional aspects in spite of the high hub/tip ratio used that have theoretically a two-dimensional flow aspects [13].

References

- [1]-Anderson, D.A., Tannehill, J.C. and Pletcher, R.H., "Computational Fluid Mechanics and Heat", Hemisphere Publishing, New York, 1984.
- [2]-Peter Stow, "Turbomachinery Blade Design using advance Calculation Methods", proceedings of NATO, ASI series, Vol.11, 1985.
- [3]-Ahmed J. Hamad, Asim H Yousif and Shokat J. Kadhm, "Computer Aided Design of Supersonic Flow Single Stage Impulse Turbine with High Work Output", Proc of the MCE 3rd ENG.SCI.Con.2000.
- [4]-Dawes, W.N., "Computational Methods in Turbomachinery", J. Mech. E. Con., Univ. of Birmingham, April 1984.
- [5]-Kostyuk, A. and Frolov, V., "Steam and Gas Turbines", Mir Publishers, Moscow, 1988.
- [6]-Talib, Z.F., "The effect of tip leakage, back swept blades and inlet distortion on centrifugal compressor flow"; PhD Thesis, Dept. of Mech. Eng., University of Liverpool, 1989.
- [7]-Arts, J., "Calculation of the Three Dimensional, Steady, Inviscid Flow in a Transonic Axial Turbine Stage", J. of Eng. GT & Power, Vol. 107, Apr. 1985.
- [8]-Sudad, I. Al-Khairi, "The effect of inlet distortion flow on the axial compressor flow field"; Msc Thesis, Dept. of Mech. Eng., Military College of Engineering Oct. 1995.
- [9]-Denton, J.D., "An Improved Time-Marching Method for turbomachinery Flow Calculation"; Trans. ASME, Vol.105, 1983, pp.514-524.
- [10]-Charles Hirsch, "Numerical Computation of Internal and External Flows"; Brussels, Belgium University, John Wiley & Sons Ltd. 1995.
- [11]-Assim, H.Y., Talib, Z.F, Ahmed, E. and Awad, M., "The prediction of Flow Behavior Through Axial Turbine Stator Blade using Numerical Solution", Eng. & Technology, No. 5, Vol.22, 2003, pp. 219-228.
- [12]-Koya, M. and Kotake, S., "Numerical Analysis of Fully Three-Dimensional Periodic Flows Through a Turbine stage"; ASME J. of Eng. for Power, Vol. 107, 1985, pp.945-952.
- [13]-Mattingly, J.D., "Elements of Gas Turbine Propulsion"; McGraw- Hill, Inc., 1996.

Nomenclature

- A damping factor
 a speed of sound (m/sec)
 c absolute velocity (m/sec)
 \overline{CF} spatial relaxation term

- CF_u relaxation term for axial velocity
- c_v specific heat capacity at constant volume (J/kg.K)
- \bar{D} damping term
- D_u damping term for axial velocity
- E total internal energy per unit volume
- \bar{F} spatial flux operator
- i,j,k,n grid indices in the x, y, z and t directions respectively
- M flux of momentum
- p static pressure (N/m²)
- r radius (m)
- r radius (m)
- t time (sec)
- u axial velocity component (m/sec)
- v blade-to-blade velocity component (m/sec)
- w spanwise velocity component (m/sec)
- W absolute velocity for stator, relative for rotor (m/sec)
- x,y,z Cartesian co-ordinates
- Δl spatial mesh size in x-direction
- Δt time step (sec)
- Δvol volume of the cell (m³)
- g ratio of specific heat of gas.
- Ω angular velocity of passage rotation (rad/sec)
- ρ density (kg/m³)

Subscripts

- o stagnation condition
- r relative for rotor, absolute for stator

Abbreviation

- CFD Computational Fluid Dynamics
- CFL Courant-Friedrichs-Lewy
- CPU Central Processor Unit

Table (1) Dimensional and flow data of the turbine stage

| | | Stator | Rotor |
|---|------|----------------------|-------|
| Chord (mm) | Hub | 43.9 | 33.9 |
| | Mid | 50.0 | 34.0 |
| | Tip | 51.4 | 35.6 |
| Maximum thickness (mm) | Hub | 6.7 | 8.4 |
| | Mid | 7.1 | 7.7 |
| | Tip | 8.2 | 6.4 |
| Chord/pitch ratio | Hub | 1.20 | 1.22 |
| | Mid | 1.29 | 1.13 |
| | Tip | 1.25 | 1.11 |
| Stagger angle (deg.) | Hub | 53.0 | 33.5 |
| | Mid | 54.0 | 37.8 |
| | Tip | 49.6 | 44.0 |
| Span height (mm) | | 45 | 45 |
| Inlet stagnation pressure (N/m ²) | | 9.36x10 ⁵ | |
| Inlet stagnation temperature (K) | | 1300 | |
| Inlet Mach number | mean | 0.21 | 0.35 |
| Inlet tangential flow angle (deg) | Hub | 0.0 | |
| | Mid | 0.0 | |
| | Tip | 0.0 | |
| Inlet radial flow angle (deg) | Hub | 0.0 | |
| | Mid | 0.0 | |
| | Tip | 0.0 | |
| Outlet static pressure (N/m ²) | Hub | 4.27x10 ⁵ | |
| | Mid | 4.06x10 ⁵ | |
| | Tip | 4.18x10 ⁵ | |
| Outlet tangential relative flow angle (deg) | mean | 71.0 | 64.3 |
| Outlet relative Mach number | mean | 1.05 | 0.82 |
| Number of blades | | 62 | 68 |

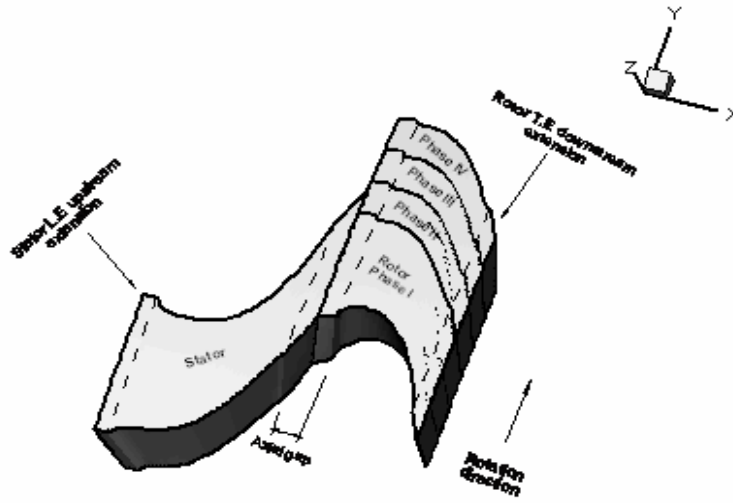


Figure. (1) 3-D view of the axial flow turbine computational domain

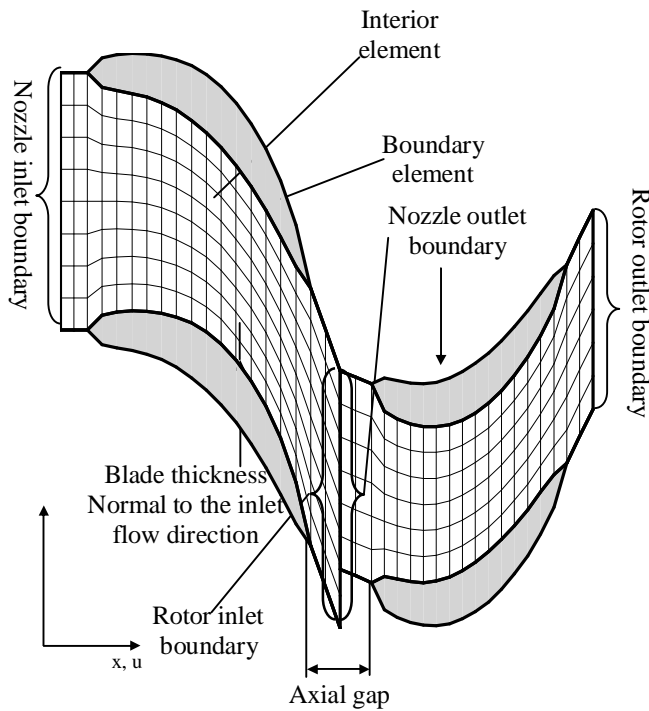


Figure (2) Blade-to-blade computational grid network

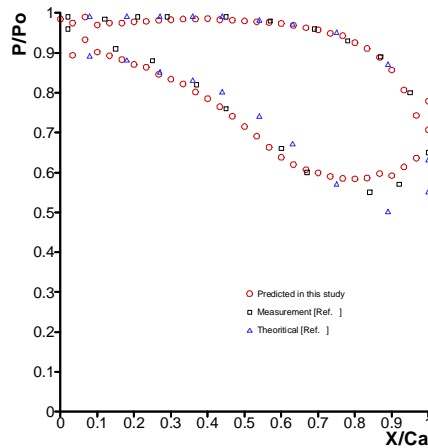


Figure (3) Comparison of predicted pressure distribution at 50% span height of the stator with that measured and calculated by Ref. [12]

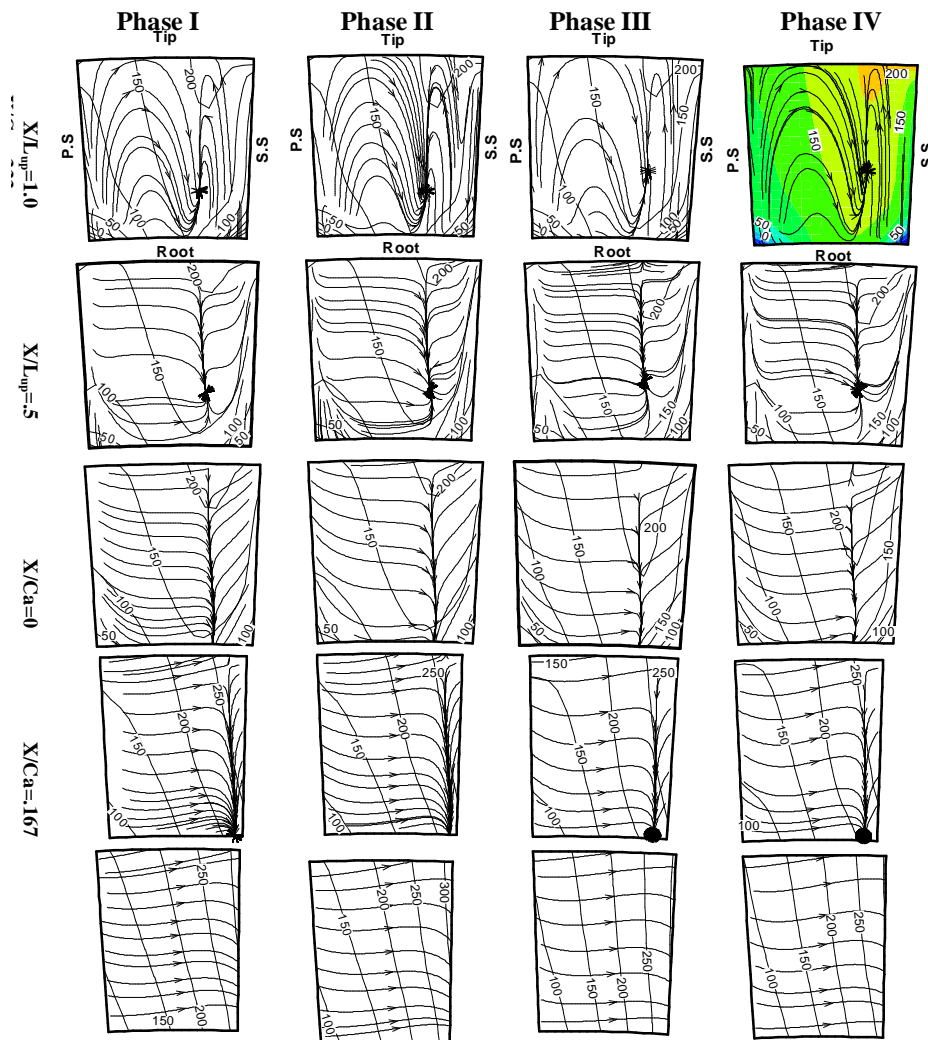


Figure (4) stator passage axial velocity contours (m/sec) with stream traces

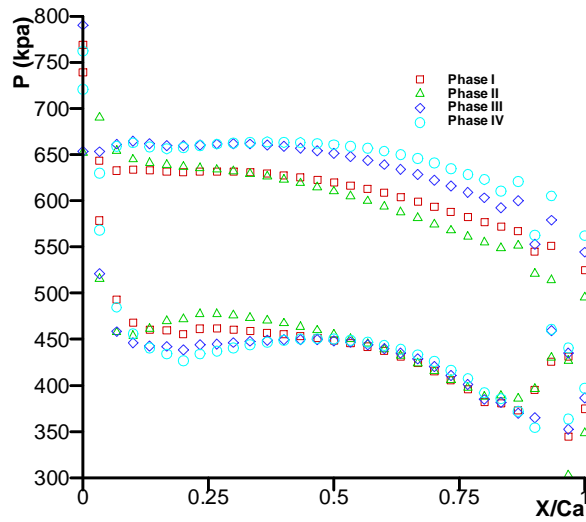


Figure (6) Periodic static pressure distribution at 50% span height of the rotor passage according to the phase location